Experimental investigations on the scattering in the post cracking tensile behaviour of UHPFRC

Philipp Hadl, Hoang Kim, Nguyen Viet Tue
Institute of Structural Concrete, Graz University of Technology, Austria

This contribution presents experimental research on scattering in post cracking tensile behaviour of Ultra-High Performance Fibre Reinforced Concrete (UHPFRC). The main objective of this work is to determine the main influence factors for scattering in post cracking tensile behaviour. The experimental programme includes 8 series of four-point bending tests, 48 specimens in total, varying the cross-sectional geometry, steel fibre type and fibre content. Each test series consists of 6 specimens. In order to exclude influences caused by the production and casting of UHPFRC, the specimens of each series were always cast in a continuous beam (length 4.2 m) and cut out later.
To gather information on the fibre orientation and distribution, slices were cut from each specimen after its bending test. By using an opto-analytic method it was found that the detected number of fibres in the section varies widely among all specimens, while the fibre orientation is very uniform.
The results of the experimental programme show decreasing scattering with increasing fibre content and cross-section area.

Keywords: UHPFRC, scattering, tensile behaviour, self-compacting, bending test

1. Introduction

The post cracking tensile behaviour of UHPFRC is assumed to scatter widely, as demonstrated in several different investigations, e.g. (Gröger et al., 2012; Leutbecher, 2012; Fehling et al., 2013). In bending test series, deviations of ± 30% are common. In Leutbecher, 2012 and Fehling et al., 2013 the large scattering was found to result from both an inhomogeneous fibre distribution and orientation. Recent research efforts have focused mainly on the fibre orientation and its effective control. Different methods for positively influencing the fibre orientation had been developed, although their practical application was limited due to challenging and/or costly requirements.

However, new studies indicate that the main reason for the large scattering is the inhomogeneous fibre distribution. The fibre orientation in a component is nearly uniform and scatters only within a small range.

To enable an effective structural design with UHPFRC, which requires a precise specification of the scattering to define reasonable safety factors as well as correct characteristic material parameters, extensive experimental investigations were carried out at Graz University of Technology, Austria. In this contribution, the experimental results are presented and discussed.

2. Experimental Investigations

The experimental programme consisted of four-point bending tests of 8 series with 6 specimens each. All 48 specimens had a length of 0.7 m but two different kinds of cross-sections. Type A represents thin plate elements with a height of 0.05 m and a width of 0.2 m; type B represents quadratic cross sections of 0.15 x 0.15 m (standard beam according to the German guideline for fibre concrete). Two cross-sections were chosen in order to compare thin elements with

standardised cross-dimensions. Within this setup, two kinds of straight steel fibres (type 1 l/d = 13/0.2 mm; type 2 l/d = 20/0.2 mm) and two fibre contents (0.75 vol.% and 1.5 vol.%) were also investigated.

Each test series consisted of 6 specimens which were always cast in a continuous 4.2 m long piece and cut out later. Such a procedure makes it possible to exclude further influences on the scattering which may result from the production of the UHPFRC and the casting process. Four point bending tests were performed with all specimens. To gather information on the fibre orientation and distribution of the tested specimens, slices were cut from each specimen after the bending test. The number of fibres and the fibre orientation were determined using an opto-analytic method.

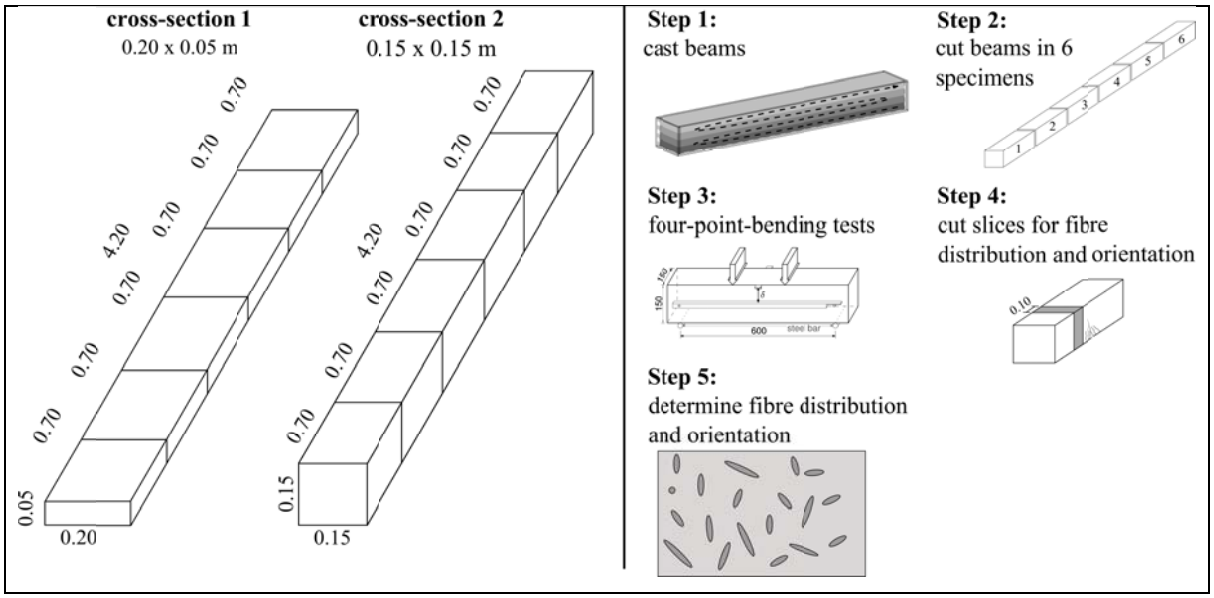

Figure 1. Cross-section of beams and schematic test setup

After mixing the plain concrete, fibres were added continuously by a fibre dosage machine. The fibre addition was carried out carefully, since this has a strong impact on the fibre distribution (see Hadl et al., 2015b). During casting, the fibre distribution hardly changes.

All 4.2 m long beams were cast in layers. Each mixture had a high flowability with spread values above 800 mm, so that self-consolidating and good release of entrapped air due to layer wise placement was maintained without compacting. This ensures a uniform fibre distribution along the beams. Subsequent to casting, the free concrete surface was covered with a plastic sheet for 24 hours. Afterwards, the beams were demoulded, cut and cured in an air conditioned (20°C) room until the test day, which occurred after 28 days.

Further, samples of cubic and cylindrical form were produced in parallel to determine the compressive strength as well as the elastic modulus for each type of concrete.

2.1. Compressive tests

As expected, the different fractions of steel fibres did not have a significant influence on the compressive strength. The cubic compressive strength was tested to $f_{c,cube} \approx 190$ N/mm² and the cylindrical strength to $f_{c,cyl.} \approx 185$ N/mm² for all series. The elastic modulus was tested to $E_c \approx$

55000 N/mm², at which a slight increase of E_c caused by increasing fibre content was observed, as can be seen in Table 1.

Table 1. Properties of hardened concrete

		M1	M2	M3	M4
fibre content	[vol.%; kg/m³]	0.75; 58.9	1.50; 117.8	0.75; 58.9	1.50; 117.8
fibre type [length / diameter]	[mm / mm]	13 / 0.2	13 / 0.2	20 / 0.2	20 / 0.2
cubic compressive strength[*1]	[N/mm²]	194.1	191.8	192.2	197.8
cylindrical compressive strength [*2]	[N/mm²]	184.9	185.5	184.4	182.0
Elastic modulus [*2]	[N/mm²]	54100	55700	54300	55800

[*1] average of 6 specimens; [*2] average of 3 specimens

2.2. Bending tests

All 12 specimens of both investigated concrete types, 6 thin specimens and 6 standardised specimens, were tested at a concrete age of 28 days. Before testing, the free concrete surface of the thin plates was grinded by a grinding machine. The standardised specimens were rotated by 90° so that what was the top surface during casting became the side surface during testing. The specimens were supported by steel bars to ensure low horizontal forces due to support friction. The four point bending test setup used in this research and the experimental procedure correspond to the German guideline for fibre concrete (DAfStb, 2009).

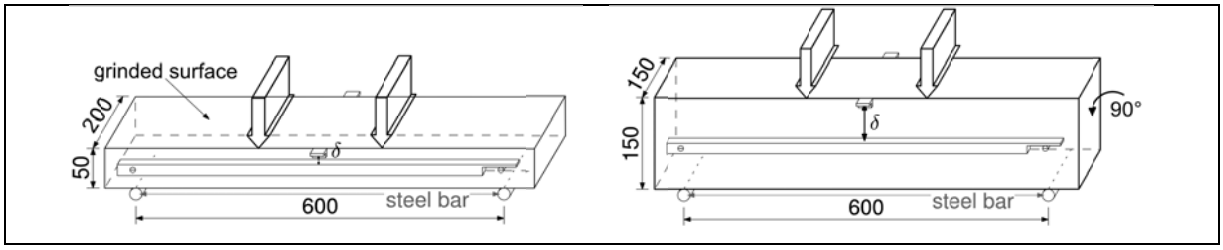

Figure 2. Thin (left) and standardised (right) specimen and test setup

The equivalent flexural strength – mid-span deflection relationship for all specimens – is given in Figure 3 and 4 with special regard to the investigated UHPFRC mixtures (M1 - M4). The variation coefficient of the flexural behaviour is depicted for each mixture in the aforementioned figures. All bending tests, no matter whether for thin plates or for standardised beams, result in deflection hardening behaviour. This applies to all investigated UHPC mixtures (M1 – M4).
In the case of thin plates (Figure 3) with the addition of 0.75 vol.% 13 mm fibres (M1), the flexural tensile strength was reached at 13 N/mm², which is within the area of the flexural tensile matrix strength (≈ 12 N/mm²). M2 with 1.50 vol.% enables strengths up to 19 N/mm². The maximum flexural tensile strength with 20 mm fibres is 18 N/mm² (M3) and 25 N/mm² (M4).

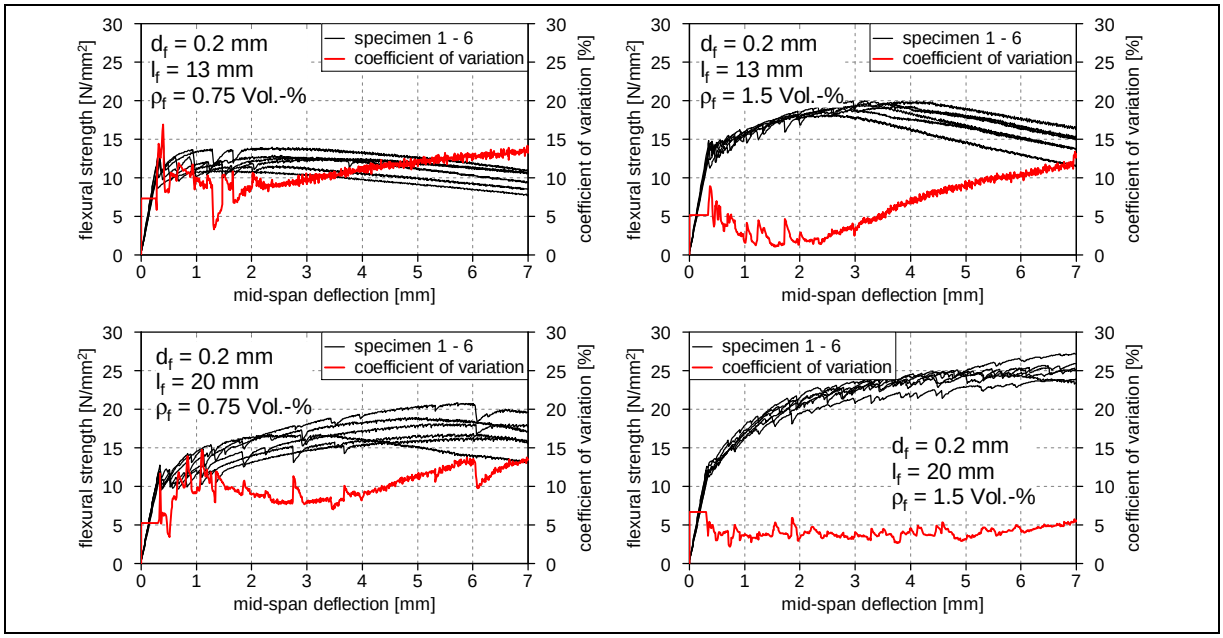

Figure 3. Flexural strength of thin plates with a cross section of 0.05 x 0.2 m (M1 – M4)

The standardised beams (Figure 4) with addition of 0.75 vol.% 13 mm fibres (M1) enable a maximum flexural strength of 12 N/mm², with 1.50 vol.% 13 mm fibres (M2) enabling a maximum flexural strength of up to 20 N/mm². 20 mm fibres enable average load bearing capacities of 18 (M3) and 23 N/mm² (M4).

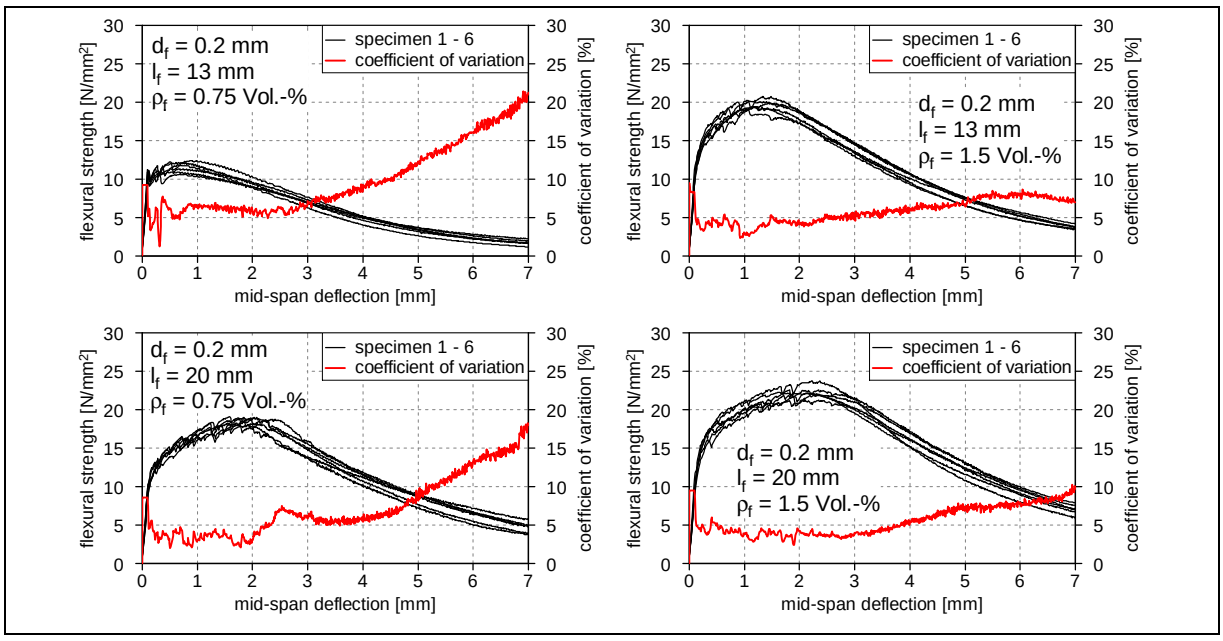

Figure 4. Flexural strength of standardised beams with a cross section of 0.15 x 0.15 m (M1 – M4)

Table 2 summarises the scattering of the investigated flexural parameters of all mixtures. The average value σ_{max} and the coefficient of variation ϑ_{max} are shown for the equivalent flexural tensile strength at load maximum. Further, the average flexural tensile strength $\sigma_{0.5/3.5}$ and the coefficient of variation $\vartheta_{0.5/3.5}$ are shown at 0.5 mm and 3.5 mm mid-span deflection according to (DAfStb, 2009).

Table 2. Statistical analysis of bending tests.

		thin plates (h = 0.05 m; w = 0.20 m)				standardised beams (h = 0.05 m; w = 0.20 m)			
		M1	M2	M3	M4	M1	M2	M3	M4
σ_{max}	[N/mm²]	12.9	19.2	17.9	25.6	11.6	19.8	18.7	22.3
ϑ_{max}	[%]	8.5	3.4	9.5	4.8	5.3	2.8	1.8	3.7
$\sigma_{0.5}$	[N/mm²]	11.1	13.5	11.3	13.1	11.3	17.0	14.3	17.8
$\vartheta_{0.5}$	[%]	8.0	6.9	3.7	3.0	6.2	4.4	2.6	4.8
$\sigma_{3.5}$	[N/mm²]	11.9	18.7	16.7	22.9	5.8	11.9	12.8	18.2
$\vartheta_{3.5}$	[%]	9.9	4.9	7.1	4.0	7.4	5.7	5.4	4.2

The statistical analysis demonstrates that thin plates lead to a slightly higher maximum bearing load than standard beams. The load bearing capacity rises with increased fibre content. This effect is even more distinct when using fibres of 13 mm instead of fibres of 20 mm. Apparently, the maximum fibre dosage is already reached when using 20 mm fibres. Further, Table 2 demonstrates that the coefficient of variation for all test series is within the range of 3 – 10 %. This indicates a very homogeneous fibre distribution, which was achieved using the fibre dosage machine. Furthermore, the scattering of the test results is decreased by increasing fibre content and cross section area. However, longer fibres lead to higher equivalent bending strength and lower coefficient of variation. Note, this conclusion is only valid as long as the failure mechanism is primarily controlled by fibre pull-out.

2.3. Fibre orientation and distribution

In order to gather information on the fibre orientation and distribution, slices were cut from each specimen after its bending test. Each slice had a width of 5 cm, and both fibre distribution and fibre orientation were determined using an opto-analytic method (Tue et al., 2007) on both cutting surfaces. After sawing, the cutting surfaces were prepared using a wet and a dry grinding method, in order to restore the generally elliptically shaped fibre cross-sections. By post-processing, closely spaced fibres that melted as a result of the high thermic and mechanical stresses during sawing were separated again. Figure 5 shows cut surfaces including fibres and created ellipses according to computer supported opto-analytic analysis.

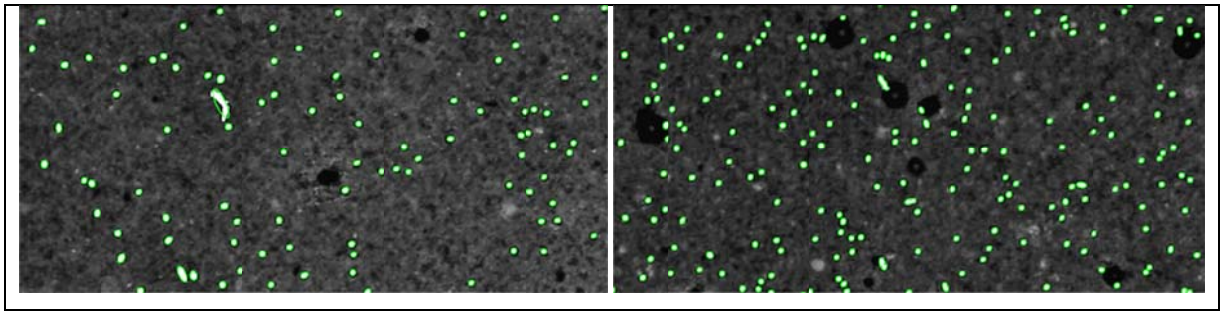

Figure 5. Sectional area with created ellipses including 0.75 vol.% (left) and 1.50 vol.% (right) of fibres

In order to describe the fibre orientation, the fibre orientation factor η was defined as the ratio of the projected fibre length in considered tensile stress direction to the real fibre length. When considering fibres, which are not evident in the section, but in the volume, one must distinguish between the fibre orientation in the section η_S and the fibre orientation in the component η_V, as described in Freytag, 2014 and Hadl et al., 2015a. The average fibre orientation in the section η_S can be determined by equation 1, where m is the number of fibres in the cross-section, $d_{F,i}$ is the length of the minor ellipse major axis (fibre diameter) and $d_{F2,i}$ is the length of the larger ellipse major axis (Schönlin, 1988).

$$\eta_S = \frac{1}{m}\sum_{i=1}^{m}\frac{d_{F,i}}{d_{F2,i}} \tag{1}$$

The fibre orientation η_V in a specific volume with a depth of lf can be calculated by equation 2, where m is the number of fibres in the cross-section and $\eta_{S,i}$ is the fibre orientation of a single fibre in the section (Freytag, 2014).

$$\eta_V = \frac{m}{\sum_{i=1}^{m}\frac{1}{\eta_{S,i}}} \tag{2}$$

Figure 6 and Table 3 show the results of the opto-analytic analysis. The fibre content ρ_f is calculated by Hilsdorf's equation (Hilsdorf et al., 1985), where A_f is the fibre cross section and Ac is the concrete surface:

$$\rho_f = \frac{m \cdot A_f}{A_c \cdot \eta_V} \tag{3}$$

The fibre orientation η_S and η_V scatter only in a low range ($\vartheta_{\eta,S} \approx 2$ - 5 %; $\vartheta_{\eta,V} \approx 3$ – 5 %) within a test series, demonstrated in Figure 6 and Table 3. In thin plates, the fibre orientation in the section (η_S) is between 0.69 and 0.82 and between 0.64 and 0.76 within the component (η_V). Using standardised beams, the fibre orientation in the section is between 0.65 and 0.77 and between 0.58 and 0.67 in the component. As expected, the fibre orientation factor decreases when the height of the specimen is increased. This effect is stronger when using longer fibres.

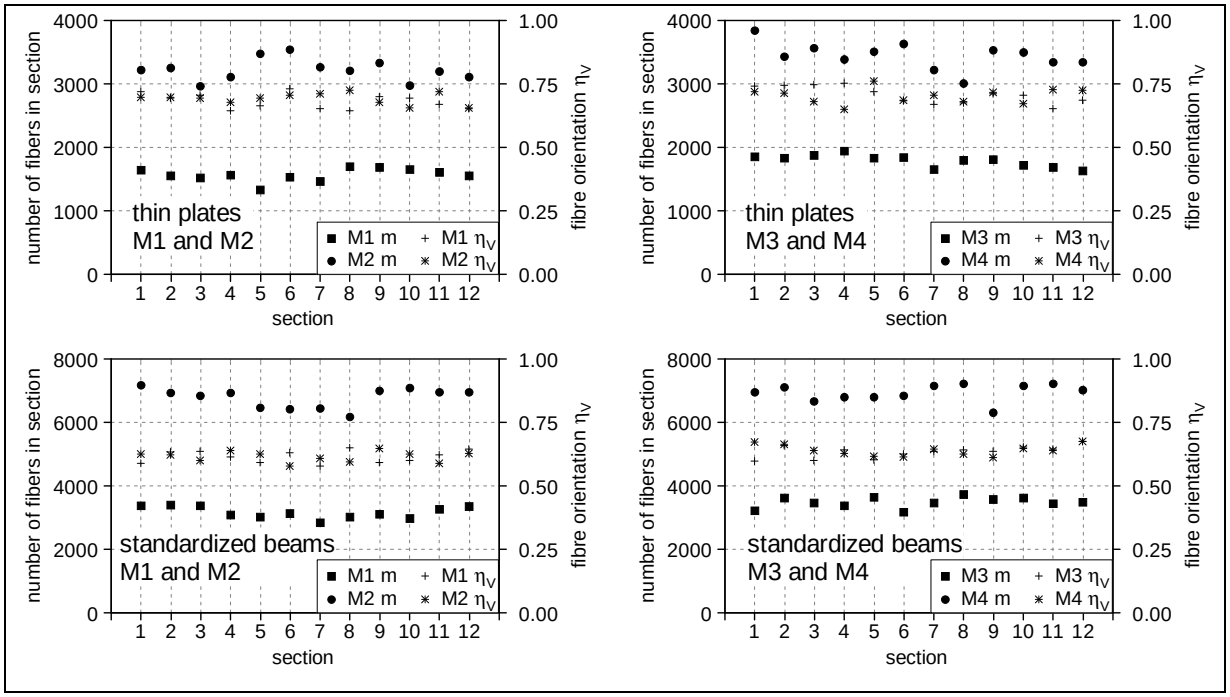

Figure 6. Number of fibres and fibre orientation in different sections (1 – 12)

Table 3. Statistical analysis of fibre orientation η_S or η_V, number of fibres m in a cross-section and calculated fibre content ρ_f (whereby μ is the mean value and ϑ the coefficient of variation of a tests series).

			thin plates (0.20 m x 0.05 m)				standardised beams (0.15 m x 0.15 m)			
			m	η_S	η_V	ρ_f	m	η_S	η_V	ρ_f
M1	μ	[N/mm²]	1563	0.77	0.68	0.72	3153	0.71	0.61	0.72
	ϑ	[%]	6.6	3.8	4.5	7.4	5.9	3.5	3.9	5.3
M2	μ	[N/mm²]	3217	0.75	0.69	1.46	6769	0.70	0.61	1.54
	ϑ	[%]	5.5	3.3	3.3	5.1	4.7	2.3	3.3	4.0
M3	μ	[N/mm²]	1786	0.76	0.71	0.80	3475	0.72	0.63	0.77
	ϑ	[%]	5.4	4.0	4.8	3.7	4.8	4.8	3.8	5.1
M4	μ	[N/mm²]	3440	0.75	0.70	1.54	6929	0.72	0.64	1.52
	ϑ	[%]	6.1	3.4	4.4	6.9	3.9	3.6	3.4	3.8

Table 3 and Figure 6 also demonstrate that the number of fibres in section m and the calculated fibre content ρ_f scatter in a larger range ($\vartheta_m \approx 4$ - 7 %; $\vartheta_{\rho f} \approx 4$ - 8 %) within a test series. In thin plates with low fibre content (0.75 vol.%; M1 & M3), the number of fibres is between 1323 and 1940, and with higher fibre content (1.5 vol.% M2 & M4) the number of fibres is between 2956 and 3834. When using standardised beams with low fibre content (0.75 vol.%; M1 & M3), the number of fibres is between 2827 and 3723 and with higher fibre content (1.50 vol.%; M2 & M4) the number of fibres is between 6163 and 7217. The scattering in the calculated fibre content (equation 3) is within the range of the scattering in the number of fibres. Furthermore,

the scattering in the number of fibres and the calculated fibre content decrease with increasing fibre content. In addition to this, longer fibres lead to a lower scattering and thus, to a lower coefficient of variation.

3. Discussion

In general, the results of the 4 point bending tests show in all cases that the scattering in the post cracking tensile behaviour can be reduced by appropriate fibre addition during the mixing process. So far, the type of fibre addition was not important. This leads to the conclusion that the scattering can be reduced significantly by appropriate fibre addition.

Furthermore, the fibre orientation in a beam is very uniform when all specimens are manufactured in a continuous process. In contrast, the number of fibres in a section and the calculated fibre content scatter more strongly. To conclude, the observed scattering in flexural behaviour is mainly caused by an inhomogeneous fibre distribution.

The distribution of fibres changes from section to section. Two parallel sections usually show different numbers of fibres. The results of the opto-analytic analysis demonstrate that there is no correlation between the detected fibre number and orientation with the observed flexural behaviour of a specimen. Therefore, the structural behaviour of a beam cannot be predicted by the number and orientation of the fibres in a section next to a macro crack.

Furthermore, the scattering in the bending tests correlates with the scattering of the calculated fibre content ρ_f within a test series. Figure 7 shows the relationship between the scattering of the fibre content ρ_f and the scattering of the bending tests ϑ_{max}, $\vartheta_{0.5}$, $\vartheta_{3.5}$ (see Table 2).

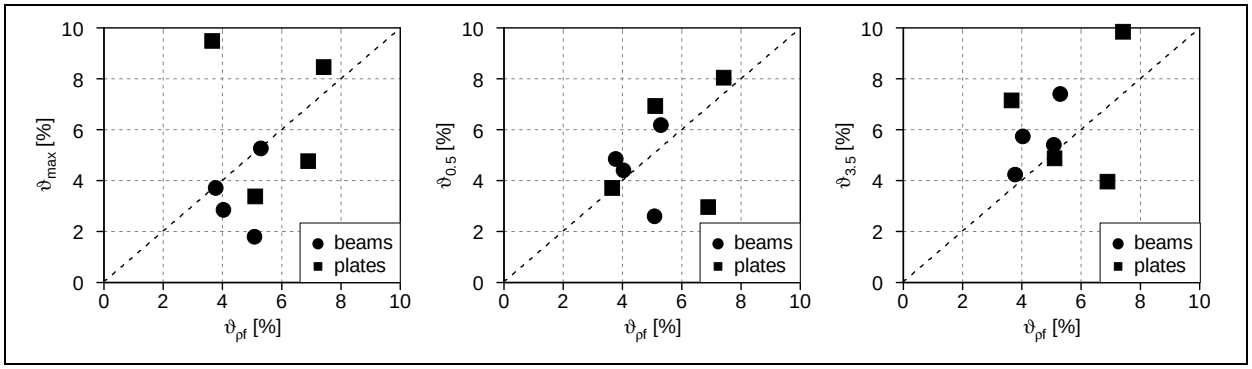

Figure 7. Correlation of scattering achieved by bending tests and opto-analytic analysis.

It is remarkable that, with an increase of the fibre content and cross-section area, the scattering in the bending behaviour and in the number of fibres as well as in the calculated fibre content decreases. Figure 8 shows that the scattering in bending behaviour and fibre content decreases when the average number of fibres in the section increases. Similar conclusions have also been reached by other researchers, such as (Erdem, 2002) and (Lingemann et al., 2013).

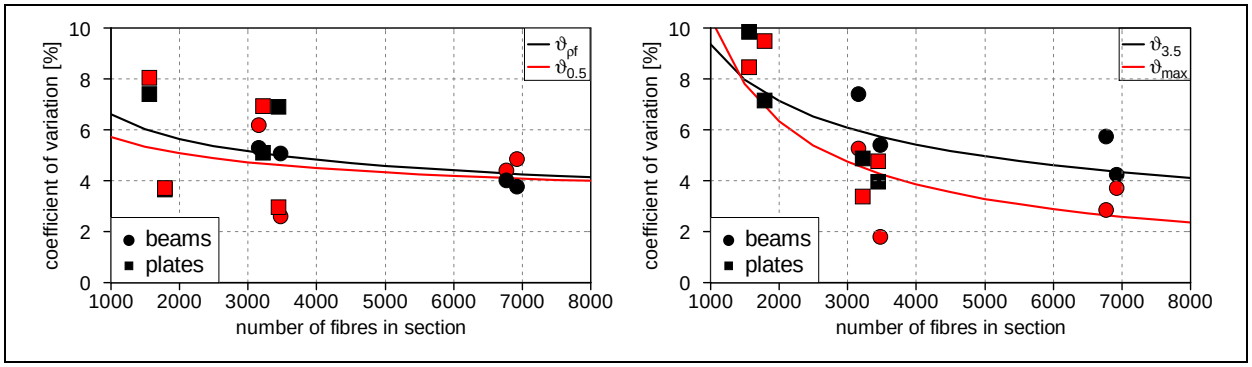

Figure 8. Decreasing scattering by increasing average number of fibres in a section.

4. Conclusions

This paper presents experimental investigations on the scattering in the post cracking tensile behaviour of UHPFRC. An extensive experimental programme was conducted, including 4 point bending tests as well as fibre orientation and distribution analysis of all tested specimens. By producing all specimens of each series in a continuous beam (length 4.2 m), from which they were cut out later, further influences on the scattering which may result from the production of the UHPFRC and the casting process, were excluded.

The results of the bending tests demonstrate that the scattering can be reduced by appropriate fibre addition during the mixing process. Furthermore, the scattering can be decreased by increasing fibre content and increasing cross-section.

The analysis of the fibre orientation and distribution showed that the fibre orientation scatters only in a low range, while the fibre distribution still scatters significantly. Based on this, it can be concluded that the scattering in the post cracking tensile behaviour of UHPFRC is mainly caused by an inhomogeneous fibre distribution. However, longer fibres lead to lower scattering.

5. References

DAfStb, Richtlinie Stahlfaserbeton, Berlin, 2009.

Erdem, E., "Probabilistisch basierte Auslegung stahlfasermodifizierter Betonbauteile auf experimenteller Grundlage", PhD-Tesis, Ruhr University Bochum, 2002.

Fehling, E., Schmidt, M., Walraven, J., Leutbecher, T., Fröhlich, S., "Ultrahochfester Beton", Betonkalender, 2013, pp. 118-239.

Freytag, B., "UHPC im konstruktiven Ingenieurbau", Habilitationsschrift, Graz University of Technology, 2014.

Gröger, J., Tue, N.-V., "Bending Behaviour and Variation of flexural Parameters of UHPFRC", *Proceedings of Hipermat 2012 3rd International Symposium on UHPC and Nanotechnology for High Performance Construction Materials*, Ed., Schmidt, M., Fehling, E., Glotzbach, C., Fröhlich, S., and Piotrowski, S., Kassel University Press, Kassel, Germany, 2012.

Hadl, P., Gröger, J., Tue, N.-V., "Experimentelle Untersuchungen zur Streuung im Zugtragverhalten von Stahlfaserbeton", *Bautechnik*, Vol. 92, 2015, pp. 385-393.

Hadl, P., della Pietra, R., Kim, H., Tue, N.-V., Pilch, E.: "Anwendung von UHPC als direkt befahrener Aufbeton bei der Integralisierung eines bestehenden Brückenbauwerks in Österreich", *Beton- und Stahlbetonbau*, Vol. 110, 2015, pp. 162-170.

Hilsdorf, H., Brameshuber, W., Kottar, R., "Abschlussbericht zum Forschungsvorhaben Weiterentwicklung und Optimierung der Materialeigenschaften faserbewehrten Betons und Spritzbetons als Stabilisierungselemente der Felssicherung", University of Karlsruhe, 1985.

Leutbecher, T., "Rissbildung und Zugtragverhalten von mit Stabstahl und Fasern bewehrtem Ultrahochfesten Beton (UHPC)", PhD-Thesis, TU Kassel, 2012.

Lingemann, J., Zilch, K., "Einfluss der Bauteilgröße auf das Tragverhalten von Stahlfaserbeton", *Bauingenieur*, Vol. 88, 2013, pp 518-524.

Schönlin, K., "Ermittlung der Orientierung, Menge und Verteilung der Fasern in faserbewehrtem Beton", *Beton- und Stahlbetonbau,* Vol. 83, 1988, pp. 168–171.

Tue, N.-V., Henze, S., Küchler, M., Schenck, G., Wille, K., "Ein optoanalytisches Verfahren zur Bestimmung der Faserverteilung und -orientierung in stahlfaserverstärktem UHFB", *Beton- und Stahlbetonbau*, Vol. 102, 2007, pp. 674-680.